Engineering an active extracellular medium with DNA programs

Marc Van Der Hofstadt,* Jean-Christophe Galas,* and André Estevez-Torres*

Sorbonne Université, CNRS, Institut de Biologie Paris-Seine (IBPS), Laboratoire Jean Perrin (LJP), F-75005, Paris, France

E-mail: marcvdhs@gmail.com; jean-christophe.galas@upmc.fr; andre.estevez-torres@upmc.fr

Abstract

Synthetic biology controls cell behaviour by engineering chemical reaction networks inside the cell. Here, we explore an alternative approach consisting in engineering reaction networks outside the cell that allow to control the chemical composition inside the cell. We do so by devising an active and programmable extracellular medium where human cells can grow and enzyme-based DNA molecular programs are functional. In particular, we demonstrate that a DNA autocatalytic network and a bistable switch remain active at 37 °C in the presence of living cells, illustrating that DNA detection down to 100 pM is possible in this context. Finally, we construct an internalization program that is capable of controlling the delivery of fluorescent DNA inside living cells. The program remains functional for 48 h and responsive for at least 6 h. We foresee that active extracellular media could be advantageously applied to *in vitro* biomolecular tracking, and further benefit tissue engineering or smart bandages.

Keywords

Synthetic biology, out-of-equilibrium, DNA nanotechnology

Living organisms adapt to dynamic environments by responding to external stimuli in a programmed manner. The majority of these stimuli correspond to changes in the chemical composition of the extracellular medium, which are transduced into reaction cascades inside the cell to activate or inhibit specific traits. Archetypal examples of extracellular cell stimulation are observed during embryogenesis[1] and wound healing,[2] where heterogeneous morphogen gradients drive morphogenesis and cell differentiation.

Synthetic biology has employed these chemical transducers to drive relatively complex *intracellular* genetic circuits[3] using simple extracellular inputs (such as small molecules[4,5] or light[6]), resulting, for instance, in the control of cellular fate[7] and intracellular composition.[8] In these approaches, the engineering efforts have been focused inside the cells. However, one may imagine a complementary route where a careful design of the *extracellular* medium controls the intracellular composition. Such strategy could be advantageously applied in tissue engineering[9] or smart bandages,[10] but also to better understand cells' behaviour in a changing environment.[11]

In this work, we illustrate this second approach by designing a culture medium where living cells can grow and chemicals react in a programmable way: extracellular reactions autonomously control the concentration of selected chemicals and, ultimately, induce a change in the intracellular composition of living cells. To do so, we take a pharmacological approach that focuses the design efforts on the reactivity of the extracellular chemicals, and that has recently revisited with the tools of DNA nanotechnology and molecular programming.[12] Indeed, extracellular DNA nanostructures have been used for delivering payloads *in vitro*[13] and *in vivo*,[14] for controlling cell adhesion,[15] and for intracellular detection.[16] In addition, nucleic acid molecular programs are able to classify cells depending on the biomarkers displayed on their surface[17–19] and are functional inside cells.[20,21] However, to our knowledge, these methods have not yet been able to dynamically control the composition of the extracellular medium in the presence of viable cells. Efforts in this direction have recently been accomplished using cell-free gene regulatory networks that control bacterial intracellu-

lar composition.[22–24] Nonetheless, the computing capabilities of these extracellular programs were limited, due to the absence of feedback loops and repression reactions, and have not yet been implemented in the presence of eukaryote cells.

Here, we show that enzyme-based DNA molecular programs with non-trivial dynamics are functional in the culture medium of eukaryote cells without compromising their viability. In particular, we demonstrate that an autocatalytic amplifier and a bistable switch are active for tens of hours in the presence of living human cells. Finally, we show that these programs can trigger the internalization of fluorescently-labelled DNA and thus control the chemical composition inside living cells. The program remains functional for 48 h and responsive for at least 6 h.

A common buffer for DNA programs and living cells

The PEN DNA toolbox is a DNA programming framework that implements the three basic operations present in gene regulatory networks — activation, repression and degradation — using short DNA oligonucleotides and 3 enzymes, namely a polymerase, an exonuclease and a nicking enzyme (PEN). The use of enzymes allows the implementation of robust[25] non-equilibrium reaction networks with feedbacks,[26,27] such as oscillations,[26,28] bistability[29,30] and spatial patterns,[31,32] at the price of a certain loss in programmability.[27]

Figure 1a depicts the core element of PEN networks used throughout this work: an autocatalytic module that exponentially amplifies an oligonucleotide **A**, before reaching a steady state. Briefly, **A** is a single-stranded DNA (ssDNA), called trigger, of sequence A and length 11 nucleotides (nt). **T** is a ssDNA, called template, twice complementary to **A**, with sequence A^*–A^*, where the asterisk indicates complementarity. Upon hybridization of **A** on the 3' end of **T**, a polymerase enzyme elongates **A** until it forms a fully double-stranded DNA (dsDNA) —the elongated strand having the sequence A–A. A nicking enzyme cuts the elongated strand, generating two copies of **A**, that dissociate from **T**, and hence show exponential amplification through the net reaction A $\rightarrow$ 2A. Simultaneously, an exonuclease

enzyme selectively degrades free **A** and, after some time, the equilibration of autocatalysis and degradation rates yields a steady state where the concentration of **A**, noted [A], is constant and equal to $[A]_{ss}$. This non-equilibrium steady state is maintained until the deoxynucleotides (dNTPs) present in the solution are consumed, which takes several days.[33] Our first objective was to find common experimental conditions where PEN autocatalysis was functional and cells were viable.

The majority of PEN autocatalytic modules operate between 42-45 °C in an optimal buffer,[34] hereafter referred as *DNA buffer*. Nevertheless, standard human cell culture conditions require 37 °C and a rich medium, such as Dulbecco's modified Eagle's medium (DMEM). We thus screened different buffer compositions and found a *cell-DNA buffer* compatible with both systems (SI Section 2 and Figures S1-S4). It contained all the components of DMEM at 2-fold dilution and all the constituents of the DNA buffer at their standard concentration, except for $(NH_4)_2SO_4$, that was suppressed, and NaCl and dithiothreitol (DTT), whose concentrations were lowered, to reduce toxicity (see Table S1). In addition, the sequences of **A** and **T** were redesigned to increase the autocatalytic efficiency at 37 °C (SI Table S2 and Figure S5).

To assess the performance of the autocatalytic network in the new buffer, we first monitored its dynamics *in the absence of cells*. To do so, strand **T** had a yellow fluorophore attached to its 5' end that was quenched upon hybridization; the shift in fluorescence signal being proportional to [A] if $[A] < [T]_0$, where $[T]_0$ is the initial concentration of **T**.[29] Figure 1b shows that autocatalytic dynamics are qualitatively similar in the DNA and the cell-DNA buffers in the absence of cells, with a sigmoidal curve characteristic of PEN autocatalytic reactions,[26] and amplification times, τ, of 65 and 125 min, respectively. We attribute the slower kinetics in the cell-DNA buffer to a lower efficiency of the enzymes (Figure S6). As expected, in both cases the fluorescence signal changed little over time in the absence of PEN enzymes. Importantly, the concentration of **A** at steady state was identical in both buffers: starting from $[A]_0 = 0.5$ nM, **A** reached 400 nM, a 800-fold amplification, within

200 min (Figure S5).

We then measured the viability of living human cervix epithelial carcinoma cells (HeLa cell line) in the different buffers and in the presence or in the absence of the autocatalytic network. Trypan blue cell staining after 24 h revealed large mortality of the cells in the DNA buffer, while the mortality remained low and comparable in the cell-DNA and in the reference cell-buffer (Figure 1c). However, propidium iodide cell staining combined with flow cytometry (Figure 1d) showed that cells divided ∼4-fold slower in the cell-DNA buffer than in the cell-buffer (doubling time of 61 and 17 h, respectively). We account this to the presence of DTT that causes partial cell detachment (Figure S2) and transiently activates endoplasmic reticulum stress.[35] In summary, cell growth was slower in the cell-DNA buffer but cell death was negligible for up to 3 days.

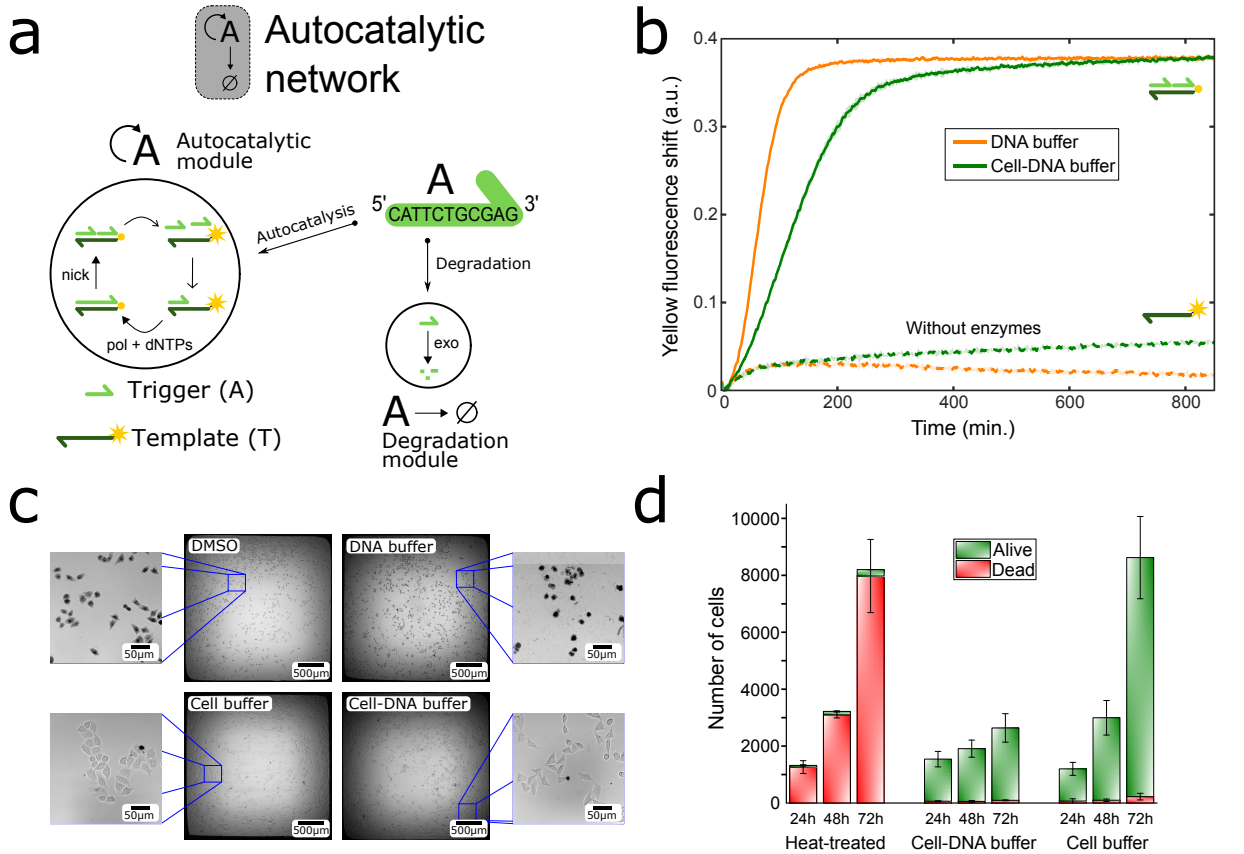

Figure 1: DNA autocatalysis is functional and cells are viable in a common buffer. a) Scheme of the core autocatalytic network used throughout this work, composed of an autocatalytic and a degradation module. ssDNAs are represented as harpoon-ended arrows. During autocatalysis, the trigger **A** replicates on template **T** through a combination of hybridization and dehybridization steps, elongation by a polymerase (pol), and cutting by a nicking enzyme (nick). Upon elongation of **A**, the fluorescent marker attached to **T** (yellow star) gets quenched. Specific degradation of **A** is carried out by an exonuclease enzyme (exo). Solid and empty arrow-heads indicate irreversible and reversible reactions, respectively. b) Fluorescence shift from the fluorescently-labelled **T** versus time for the autocatalytic network in standard DNA buffer (orange line), or in the biocompatible cell-DNA buffer (green line), at 37 °C in the absence of cells. Dashed lines correspond to negative controls in the absence of enzymes. The shades, corresponding to the standard deviation of a triplicate experiment, are of the order of the line thickness. c) Bright-field images of trypan blue-stained cells after 24 h incubation in different buffers, dead cells appear in black. Treatment with DMSO is a control for dead cells. The black halo around the central images is an optical artifact. d) Number of dead and live cells per well determined by propidium iodide staining and flow cytometry for different incubation times and conditions (experiment performed per triplicate and repeated 2 different days, $n = 6$). In panels c and d the cell-DNA buffer contained the autocatalytic network. Conditions: $[A]_0 = 0.5$ nM, $[T]_0 = 100$ nM in panel b and $[A]_0 = 20$ nM, $[T]_0 = 200$ nM in c and d.

The dynamics of DNA programs are weakly affected by living cells

It remains to be proven that PEN reactions remain active and can be reprogramed in a solution containing living cells. To do so, we quantified the dynamics of two PEN networks in the cell-DNA buffer in the presence and in the absence of cells, using the DNA-buffer in the absence of cells as a positive control. From hereafter, for biological relevance, all experiments were performed in standard 384 cell culture well plates (see Methods). Figure 2a displays the amplification onset time, τ, of the autocatalytic network as a function of the initial concentration of **A**, $[\mathrm{A}]_0$. In all three cases, τ depends linearly on $\log([\mathrm{A}]_0)$, indicating that autocatalysis followed first order kinetics. In addition, a moderate reduction in the rate of the autocatalytic reaction was observed: by 20% between the DNA and the cell-DNA buffer in the absence of cells and by a further 20% in the presence of living cells. Importantly, these data show that this DNA program was able to detect a specific DNA sequence at a concentration of 100 pM in the presence of cells, within 300 min.

The autocatalytic network can be easily reprogrammed into a bistable switch[30] by just adding a repressor strand **R**, creating a reactive system with two antagonistic stable states: an *ON* state where autocatalysis of **A** occurs and $[\mathrm{A}]_{ss}$ is high, and an *OFF* state, where the combined degradation of **A** by **R** and the exonuclease outcompetes autocatalysis, yielding $[\mathrm{A}]_{ss} = 0$ (Figure 2b). In the later, **A** binds to the ssDNA repressor **R** and is extended by the polymerase into a non-functional ssDNA, called waste $\mathbf{W_1}$, which is degraded by the exonuclease. Figure 2c shows the dynamics of the bistable switch in the presence of cells as a function of the concentration of **R**, at constant $[\mathrm{A}]_0$. Increasing $[\mathrm{R}]_0$ slows down the exponential amplification of **A** until the system switches to the *OFF* state at $[\mathrm{R}]_0 >$ 40 nM, where no amplification was detectable within 850 min. The plot of τ as a function of $[\mathrm{R}]_0$ highlights a strongly non-linear response that is characteristic of a bifurcation point (Figure 2d). In addition, it shows that less **R** is needed to switch off autocatalysis in the cell-DNA buffer than in standard DNA-buffer, in agreement with faster autocatalysis kinetics in the latter. Again, the presence of the cells does not qualitatively change the

dynamics of the bistable switch in the cell-DNA buffer. Gel electrophoresis analysis confirmed that the bistable switch produced the same products in the presence and in the absence of cells (Figure 2e), with a similar pattern to the one previously obtained in standard PEN conditions.[25]

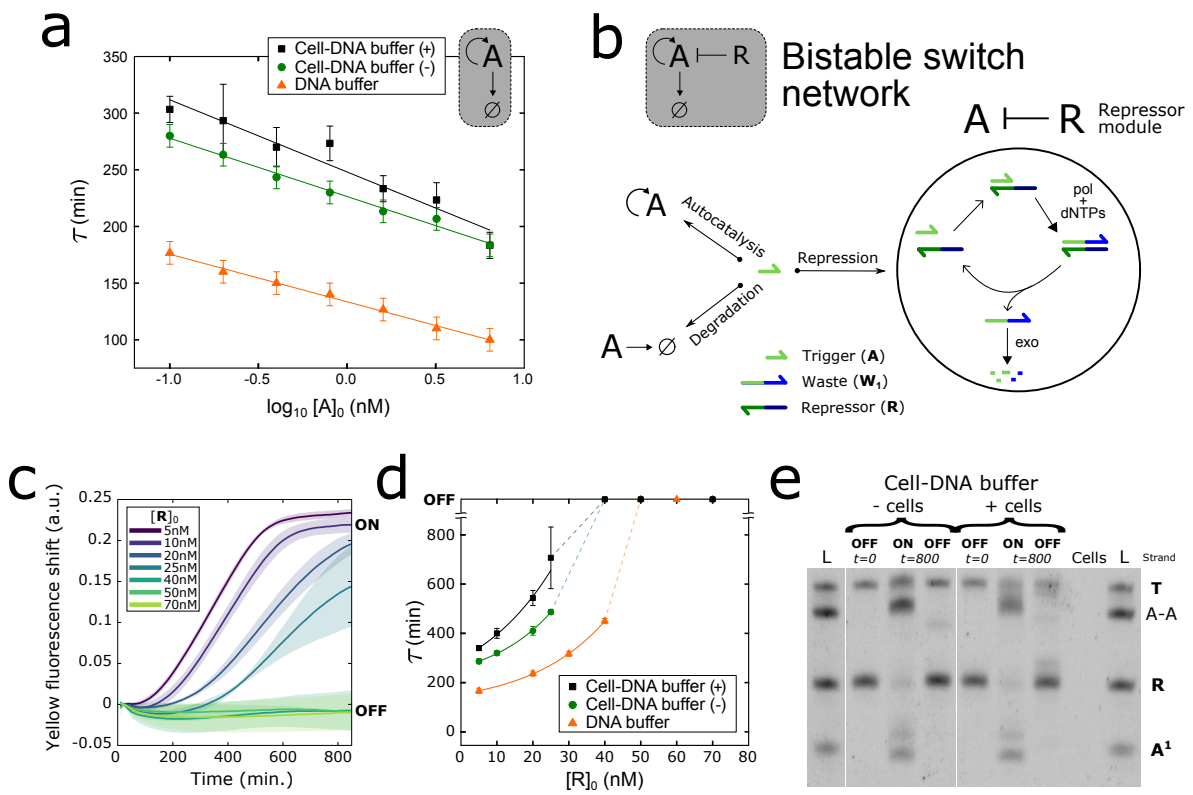

Figure 2: Dynamic enzyme-based DNA reaction networks are fully functional in the presence of cells. a) Amplification onset time, τ, against the decimal logarithm of the initial concentration of **A** for the autocatalytic network in two different buffers, and in the presence ((+), black squares) or in the absence ((-), green circles) of cells. b) A bistable switch (in gray) is obtained when the autocatalytic network is combined with a repressor module, where **A** binds to repressor **R** and is converted into a non-functional ssDNA, waste $\mathbf{W_1}$, that is degraded by the exonuclease. c) Fluorescent shift from fluorescently-labelled **T** versus time for the bistable switch in the cell-DNA buffer in the presence of cells for increasing concentrations of **R**, $[\mathrm{R}]_0$. d) τ versus $[\mathrm{R}]_0$ for the bistable switch in the same conditions as in panel a. Data determined from panel c and Figure S7. e) Denaturing polyacrylamide gel electrophoresis showing the products obtained in the *OFF* and *ON* states of the bistable switch in the absence (-) or in the presence (+) of cells, at different times. L is a ladder containing the template **T** (20 nt with a JOE fluorescent label), the strand A-A (a 22 nt resulting from the elongation of **A** on **T**), repressor **R** (15 nt) and species $\mathbf{A}^1$ (10 nt). The 'cells' lane is an extract from a solution containing cells only. Experiments were performed in 384-well cell culture plates. The error bars and the shades in panels a, c and d correspond to one standard deviation of a triplicate experiment. Solid lines in panels a and d are linear and exponential fits, respectively, while dashed lines are guides to the eye. Conditions: $[\mathrm{T}]_0 = 100$ nM in all panels, and $[\mathrm{A}]_0 = 0.5$ nM in panels c and d.

An active medium that controls cellular internalization

Until now we have shown the coexistence of two orthogonal autonomous (and programmable) systems: the cells, that are viable for at least 72 h in the presence of DNA programs, and PEN DNA reactions, which can be assembled into different reaction networks that are functional for up to 14 h in the presence of cells. We now explore the possibility of engineering extracellular DNA programs that alter the chemical composition of living cells in a programmed manner. To do so, we created an internalization switch by coupling the bistable switch just described to the conversion module $\mathbf{A} \rightarrow \mathbf{S}$, that releases fluorescently-labeled ssDNA signal **S**, later internalized by the cells (Figure 3a). The conversion module relies on the reaction $\mathbf{A} + \mathbf{C} \rightarrow \mathbf{S} + \mathbf{W_2}$, where complex **C** is a partially double-stranded DNA whose shorter top strand is **S** and whose longer bottom strand (**D**) is attached to a hydrogel bead to avoid uncontrolled internalization, hereafter termed conversion bead. **A** is designed to bind to the bottom strand of complex **C**, which is then elongated by the polymerase to form the fully dsDNA waste $\mathbf{W_2}$ and release the top strand **S** by polymerase-assisted strand displacement into the extracellular medium. Once in solution, **S** is passively internalized by living cells[36] within 2–4 hours, making them fluorescent (SI Video S1 and Figure S8). Figure 3b sketches the experimental setup, where the cells and the conversion beads were placed in the bottom of a culture well filled with an active medium containing the cell-DNA buffer and the bistable switch. The beads covered 2.6% of the well's surface and were homogeneously distributed among the well's bottom surface (SI Figure S10).

The conversion module was designed such that **A** hybridized to **C** less favourably than both to **T** and **R**, and thus **S** was released only when the bistable switch was *ON* and [A] was high (SI Figure S11). Figure 3c shows the dynamics of production of **A** and release of **S** in the medium for the internalization switch in the presence of cells in the *ON* and *OFF* states, corresponding, respectively, to $[\mathrm{R}]_0 = 0$ nM and $[\mathrm{R}]_0 = 200$ nM. In the *ON* state, **A** is amplified during at least 10 h, when it saturates **T** and causes its fluorescent signal to reach a maximum before decreasing slowly. This indicates that at $t = 10$ h, $[\mathrm{A}] \approx 2[\mathrm{T}]_0$

= 400 nM in the medium, a 20-fold amplification. At this point, there was enough free **A** to trigger the conversion reaction, releasing **S** from the bead into the extracellular medium. This process resulted in a decrease and an increase in the red fluorescence of the medium and the conversion bead, respectively, and took another 10 h. In contrast, in the *OFF* state, no amplification of **A** was observed and the release of **S** in the medium was negligible after 20 h and was at least 8-fold lower after 48 h. We remark the fact that the initial concentration of **A** (20 nM) would be sufficient for the polymerase to convert the total quantity of **C** in the well (18 nM) into **S**, but this release did not occur until [A] was high, showing the robustness of the designed conversion module. Note that the evaporation of the medium was significant during this 48 h-long experiment (30%). This could explain the long-term decrease and increase of the fluorescent signals used to follow **A** and **S** in the medium (SI Figure S12) but did not compromise the function of the DNA program.

After 48 h, the cells were rinsed to eliminate the excess of free **S** in the medium and imaged. Figure 3d clearly shows that only the cells cultured in the presence of the internalization switch in the *ON* state appear fluorescent. Higher magnification images (SI Figure S13) revealed an internalization into dot and rod-like compartments, which is compatible with an accumulation in mitochondria as observed for cyanine fluorophores[37] similar to the one attached to **S**. Note that cells became fluorescent only when **S** was labelled with certain fluorophores and not others (Figure S9). Figure 3e displays the distribution of the average fluorescent intensity per cell, demonstrating that the *ON* state results in a rate of cell internalization significantly different from the *OFF* state (two-tailed Mann-Whitney U test, p-value <0.001), with, respectively, means of 3.7 and 1.1, medians of 3.3 and 1.0 and standard deviations of 2.13 and 0.62. A negative control in the absence of enzymes produced a distribution of cellular fluorescence not significantly different to the *OFF* state, showing that the concentration of the red fluorophore inside the cells is controlled by the DNA program.

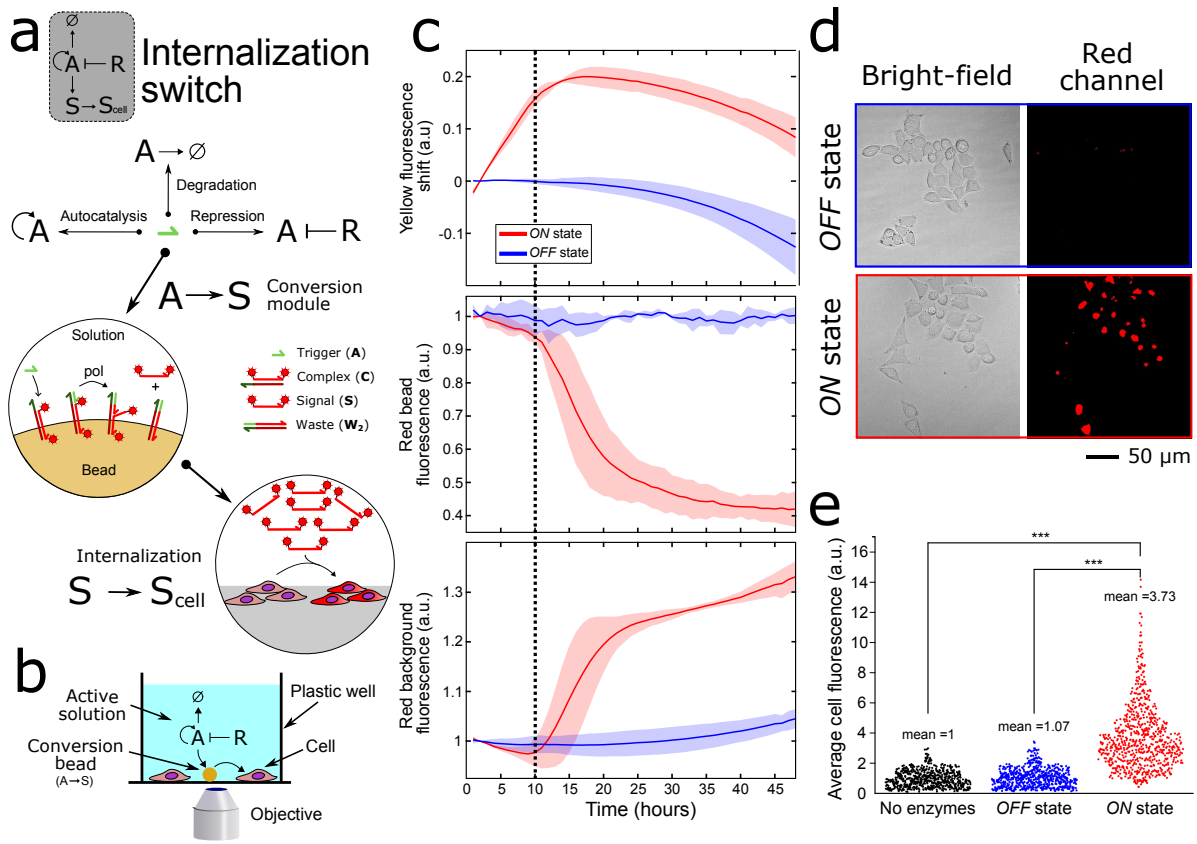

Figure 3: An active medium that controls the internalization of fluorescent DNA inside living cells. a) Scheme describing the operation of the DNA internalization switch embedded in the active medium. The gray box depicts the topology of the reaction network, composed of a bistable switch and a conversion module. In the conversion module, free **A** binds to complex **C**, attached to hydrogel beads, and is elongated by the polymerase. This causes the release of the red fluorescent strand **S** into the solution, that can be passively internalized by the cells ($\mathbf{S}_{cell}$). Red stars indicate attached red fluorophores. b) Cartoon of the experimental setup (not to scale). The cells are cultured in an active medium containing the bistable switch in solution and the conversion module attached to hydrogel beads of 34 μm diameter. c) Fluorescence versus time plots displaying the dynamics of the internalization switch in the *ON* (red line) and *OFF* (blue line) states in the presence of cells: production of **A** (top) and release of **S** from the bead (middle) into the solution (bottom). The black dashed line is a guide to the eye. d) Overlapping bright-field and red fluorescence microscopy images of living cells rinsed after being cultured for 48 h in the active medium in the *OFF* and *ON* state. e) Quantitative analysis of the average red fluorescence intensity per cell for cells cultured in the active medium in the absence of enzymes (black dots), in the *OFF* state (blue dots), and in the *ON* state (red dots). At least 649 cells were analyzed in each condition. Experiments were performed in 384-well culture plates in duplicates and repeated 3 different days ($n = 6$). The shade in panel c corresponds to one standard deviation. Conditions: $[\mathrm{A}]_0 = 20$ nM, $[\mathrm{T}]_0 = 200$ nM. The *ON* and *OFF* states correspond to $[\mathrm{R}]_0 = 0$ and 200 nM, respectively.

Since PEN reactions are maintained out of equilibrium for long periods of time, one should be able to turn an *OFF* state *ON* by adding a DNA activator, and hence trigger internalization at different times. To test this, we added either a ssDNA activator, $\mathbf{R}^*$, or a random sequence to the *OFF* state. $\mathbf{R}^*$ is complementary to $\mathbf{R}$ and, upon hybridization, it reduces $[\mathrm{R}]_0$, and hence switches the system to the *ON* state. Figures 4 and S14 show the response of the internalization switch when a 4.5-fold excess of $\mathbf{R}^*$ or of the random sequence was introduced 6 h after the beginning of the experiment, together with controls for the *ON* and *OFF* states. The switch worked as expected. No significant difference was observed in the *OFF* state after the addition of the random sequence. In contrast, the addition of $\mathbf{R}^*$ switched on the autocatalysis, which further caused the release of $\mathbf{S}$, with delays of 16 h and 13 h, respectively, compared to the *ON* state. We attribute the slower dynamics to the residual presence of $\mathbf{R}$, which slows down autocatalysis as shown in Figure 2. In addition, this demonstrates that the PEN reactions remain active for at least 35 h, since the polymerase and the nicking enzyme are required for exponential amplification and exonuclease is essential to maintain the OFF state.[30] As anticipated, only the cells where the DNA activator was introduced internalized the fluorescent strand $\mathbf{S}$ (Figure 4b) (two-tailed Mann-Whitney U test, p-value <0.001), showing that the active extracellular medium was responsive for at least 6 h and was able to change cellular composition for up to 48 h of cell culture.

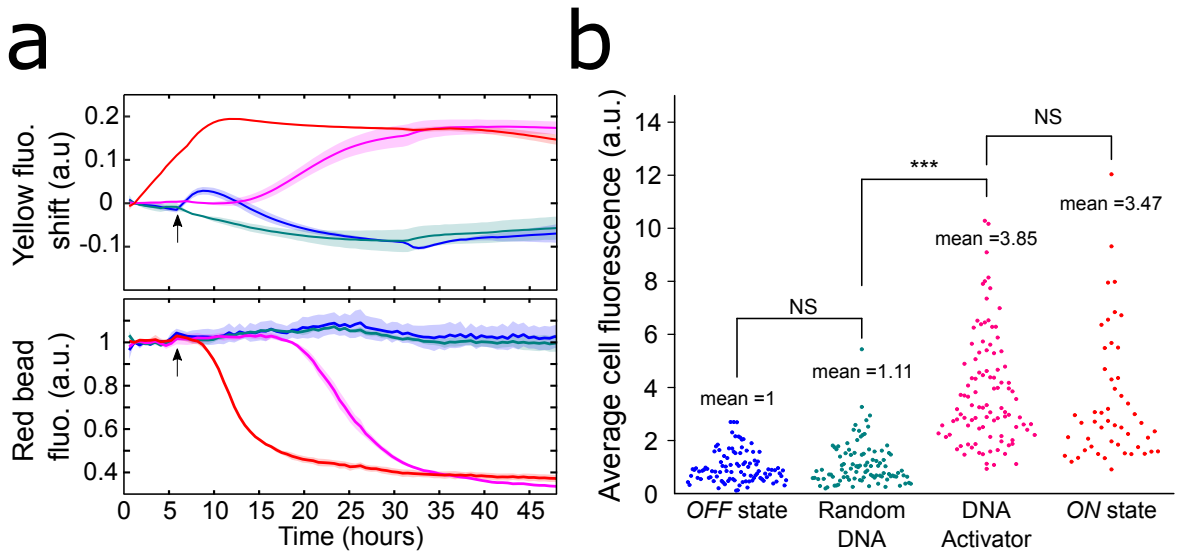

Figure 4: The internalization switch is responsive. a) Fluorescence versus time plots showing the dynamics of production of **A** (top) and the release of **S** from the bead (bottom) in the presence of cells. The curves show the unperturbed *ON* (red) and *OFF* (blue) states, as well as *OFF* states where a ssDNA, either $\mathbf{R}^*$ (pink) or a random sequence (teal), was introduced at $t = 6$ h (indicated with an arrow). b) Quantitative analysis of the average red fluorescence intensity of living cells after 48 h exposure to the conditions in panel a ($n = 50$). The shade in panel a corresponds to one standard deviation of a duplicate experiment ($n = 50$). NS: Not significant. Conditions: $[\mathrm{A}]_0 = 20$ nM, $[\mathrm{T}]_0 = 200$ nM. The *ON* and *OFF* states correspond to $[\mathrm{R}]_0 = 0$ and 200 nM, respectively and ssDNAs were added at 900 nM.

Conclusions

In this work, we have developed an active and programmable extracellular medium that is capable of exerting a basic control on the composition of living cells. To do so, we found common conditions in which an extracellular enzyme-based DNA program was functional in the presence of a viable culture of human cells. The program was encoded with PEN reactions that allow to design non-equilibrium chemical reaction networks with non-trivial dynamics. With these tools we have engineered an extracellular medium that controls the internalization of a DNA strand inside living cells. Importantly, the program remained responsive to external signals for at least 6 h.

Our method stands out for its simplicity. Non-equilibrium DNA programs could be run in the presence of living cells without introducing any major modification other than a change in

the composition of a classical growth medium. In particular, no chemical modification of the DNA program, no genetic modification of the cells, nor special apparatus other than standard cell culture well-plates were needed to run the autocatalytic network and the bistable switch. Only the more complex internalization program needed the addition of hydrogel beads to physically separate the cells from the released species **S**. Remarkably, the program worked at 37 °C and without human intervention. The presence of the enzymes that continuously synthesize fresh DNA may account for the robustness of the method, although complementary approaches based on DNA strand displacement reactions may improve the programmability of the active medium.[38] In addition, the DNA programs were fast compared with cell division (3 to 7-fold), and remained active for two days, which could be possibly extended up to a week.[33] Furthermore, the wide array of reactivities offered by oligonucleotides, thanks to chemical modification or sequence selection, anticipates that the active medium developed here could receive and release a variety of inputs and outputs that can further control cellular behaviour, either genetically[39] or via aptamers.[12] Finally, PEN reactions are well suited to engineer concentration patterns that emulate those observed during early embryo development.[25,32,40]

With these properties, one foresees that DNA-based active extracellular media could be used for real-time *in vitro* detection of fast evolving or long-lasting biomarkers in living cells.[41] In addition, DNA concentration patterns self-organizing inside active media could provide novel methods to engineer tissues, with differentiation induced over space and time in a controlled manner. Finally, active media could be integrated into smart bandages[10] or engineered living materials[42] and function as a detector,[41] as an actuator, or both, while benefiting of the computation capabilities of DNA.

Methods

All DNA strands were designed heuristically and with the help of Nupack[43] and purchased from Integrated DNA Technologies, Inc (U.S.) or Biomers (Germany). The Bst DNA polymerase large fragment and the Nb.BsmI nicking enzymes were purchased from New England Biolabs, while the *Thermus thermophilus* RecJ exonuclease was produced in-house as described.[44] Unless otherwise stated, all experiments were performed at 37 °C. DNA sequences and further experimental procedures are provided in the Supplementary Information.

Monitoring of PEN DNA reactions

When cell culture conditions were not needed, the dynamics of PEN reactions were recorded in 20 μL solutions inside 150 μL qPCR tubes using a Qiagen Rotor-Gene qPCR machine or a CFX96 Touch Real-Time PCR Detection System (Bio-Rad). To calculate the fluorescence shift, the raw fluorescence intensity was normalized by an early time point ($t = 5$ min), and subtracted from 1, as done previously.[32] The onset amplification time, τ, was defined as the time point at which 50% of the fluorescence of the steady state of the *ON* state was reached. Standard experimental conditions were 8 U/mL polymerase, 100 U/mL nickase, 31.25 nM exonuclease, and 0.4 mM dNTPs (New England Biolabs). Standard DNA buffer was used as described previously,[32] and cell-DNA buffer's composition is provided in Table S1. Reference cell-buffer contained DMEM supplemented with 1% Penicillin-Streptomycin antibiotics to avoid bacterial contamination. Polyacrylamide denaturing gel electrophoresis (PAGE) at 20% was run for 2 h at 200 V in 0.5X TBE buffer, stained with 1000x Sybr Gold (ThermoFisher: S11494) for 10 min, and imaged using a Gel Doc™ EZ Gel Imager (Bio-Rad). Note that the gels indicate that the autocatalytic network produces a 10-mer strand ($\mathbf{A}^1$) in larger quantity that the expected 11-mer strand $\mathbf{A}$. We hypothesize that this behavior is due to the reactivity of the nicking enzyme. Since the region of complementarity of species $\mathbf{A}^1$ and $\mathbf{A}$ to species $\mathbf{T}$ are identical, this feature should not affect the autocatalytic

dynamics for the interest of this article.

Particle loading

Conversion beads were constituted of porous streptavidin-conjugated sepharose hydrogel beads with 34 μm average particle size (GE healthcare: GE17-5113-01) functionalized with biotinylated DNA constructs. Firstly, we annealed 290 pmoles of double-biotinylated $\mathbf{C_1}$ with 247 pmoles of **S** in a 115.7 μL 5 mM $MgSO_4$ solution with a temperature ramp of 1 °C every 10 s, from 90 °C to 20 °C. Secondly, we rinsed twice 5 μL of Sepharose solution ($\sim$10000 beads/μL) with washing buffer (10 mM Tris-HCl, pH 7.5, 1 M NaCl, 1 mM EDTA, 0.2% Tween 20), followed by a third wash with deionized water and decantation. The DNA annealed solution was mixed with the rinsed beads and immediately agitated for 10 seconds, to further incubate it at 40 °C for 30 min, with agitation to avoid particle sedimentation. Finally, the functionalized beads were rinsed three times with a 5 mM $MgSO_4$ solution to remove unbound DNA, and the final volume was adjusted to 100 μL. Functionalized beads were used at 0.62%, which accounted a low surface coverage of the wells (Figure S10).

Cell culture

Human cervix epitheloid carcinoma cells (HeLa cell line) were grown at 37 °C and 5% CO_2. The cells were firstly grown in two sequential steps (10% and 5%) of FBS (Dominique Dutscher: S1810-500) before reducing the FBS down to 2.5%, to avoid drastic shock upon removal of FBS. The adherent culture was maintained in 2.5% FBS cell-buffer medium until reaching 80-90% confluence, where cells were trypsinized with trypsin-EDTA (PAN Biotech: P10-019100) and diluted into fresh 2.5% FBS cell-buffer medium. Experiments were carried out in 384 cell well plates (ThermoFisher: 142762). 1600 cells in 50 μL of medium per well were allowed to adhere to the surface of the well for 24 h before further experimental handling.

For cell viability experiments, the medium was removed from the well and replaced with

50 μL of the buffer under test, and left for the stated number of days. For DMSO controls, 10 μL of DMSO (Panreac: A3672) was directly added from stock solution. For trypan blue viability assays, 2 μL of trypan blue 0.4% solution (Gibco: 15250061) was added and gently mixed. After 5 min in the incubator, the wells were rinsed twice with 1X PBS, always leaving some solution in the well to assure that no cells were removed during rinsing. Cells were then imaged in bright-field with a 2.5X 5324.8 μm^2 and a 20X 644.84 μm^2 objective.

For quantification of cells by fluorescent-activated cell sorting (FACS), the wells were gently rinsed with 50 μL 1X DMEM and incubated 8 minutes with 50 μL trypsin (stock solution) before inactivation with 50 μL of DMEM supplemented with 10% FBS. The cell solution was mixed with 250 μL FACSFlow (Fisherscientific: 12756528) and 0.5 μL of propidium iodide (20 mM, ThermoFisher: L7012). Heat-treated cells were left at 65 °C for 10 minutes. A Becton-Dickinson flow cytometer (FACSCalibur) equipped with a 488 nm argon ion laser was used to excite propidium iodide, and record the emissions in the fluorescence channel FL-2 (band pass 585/42 nm). Cells were quantified for 3 min at a flow of 60 μL/min. Fluorescent measurements were treated and analyzed with a home-made Matlab (The Mathworks) routine. Note: due to the presence of a reducing agent (DTT), standard MTT viability test could not be performed.

Microscopy

PEN DNA reactions and cells in 384 cell well plates were monitored using a Zeiss Axio Observer Z1 fully automated epifluorescence microscope equipped with a ZEISS Colibri 7 LED light, YFP and RFP filter sets, and a Hamamatsu ORCA-Flash4.0V3 inside a Zeiss incubation system to regulate temperature at 37 °C, in the presence of high humidity and at 5% CO_2. Note: we observed up to a 75% reduction in τ for 384 well plates (Figure 2a) than that for qPCR machines (Figure 1b), which we mainly attribute to a difference in the materials of the two containers used (polystyrene wells and polypropylene tubes respectively) and to a lower robustness of the microscope to maintain a constant temperature compared to

321 a thermocycler. Multi-color fluorescence and bright-field images were recorded every 10 min
322 (Figure 2), 35 min (Figure 4) or 1 h (Figure 3) with a 2.5X objective. To detect cellular
323 internalization, cells were rinsed twice with 60 μL of DMEM (with a 5 min incubation at
324 37 °C between rinses) and the entire well was imaged with a 4-by-4 image array using a 20X
325 objective.

326 Image and data treatment

327 The raw microscopy images were treated with ImageJ / Fiji (NIH) and Matlab. To follow the
328 dynamics of the PEN reactions, time-lapse images were imported into a stack for each well.
329 Three threshold values were defined to select the template fluorescence (yellow channel),
330 the background fluorescence and the bead fluorescence (red channel). In the case of the
331 beads, pixels were only selected if they stayed within the selection criteria for more than
332 half the duration of the experiment, to avoid disturbances caused by the movement of the
333 beads. Each thresholded image was averaged along the y axis to create an intensity profile
334 at each time point. These profiles were stacked over time into a kymograph, which was then
335 normalized by the profile of the 2nd time point to correct from inhomogeneous illumination.
336 The kymographs were then averaged over space to obtain the profiles of intensity versus
337 time. To correct from time-dependent artefacts introduced by the microscope, the profiles of
338 each well were normalized with a negative control (absence of enzymes, $n = 2$). Fluorescence
339 shifts were calculated as described above.

340 For the characterization of cellular fluorescence, and prior to combining images into the
341 4-by-4 image array, the background of red fluorescence images was subtracted using ImageJ
342 'subtract background' routine with a 2000 pixel rolling ball radius and sliding paraboloid
343 parameters. Subsequently, the mean background fluorescence was removed from the image
344 to have a homogenous background within the image array. The contour of each cell was
345 manually selected in the bright-field image and used to extract the average red fluorescence
346 of each cell. Selection of cells was restricted to the middle of the wells to avoid optical

artefacts.

Acknowledgements

We thank Stéphanie Bonneau and Ramón Eritja for supplying the cells, Clara Berenguer-Escuder for advice with cell culture, and Matthieu Morel, Yannick Rondelez and Guillaume Ginés for insightful discussions. We also thank the financial support from the European Research Council (ERC) under the European's Union Horizon 2020 program (grant no. 770940, A.E.-T.), by the Ville de Paris Emergences program (Morphoart, A.E.-T.), by a Marie Skłodowska-Curie fellowship (grant no. 795580, M.vdH.) from the European Union's Horizon 2020 program, and by a PRESTIGE grant (grant no. 609102, M.vdH.) from the European Union's Seventh Framework Programme.

Author contributions

All authors designed research, discussed the results and wrote the paper. M.v.d.H. designed and performed the experiments and analysed the data.

References

(1) Dessaud, E.; McMahon, A. P.; Briscoe, J. Pattern formation in the vertebrate neural tube: a sonic hedgehog morphogen-regulated transcriptional network. *Development* **2008**, *135*, 2489–503.

(2) Werner, S.; Grose, R. Regulation of Wound Healing by Growth Factors and Cytokines. *Physiological Reviews* **2003**, *83*, 835–870.

(3) Cameron, D. E.; Bashor, C. J.; Collins, J. J. A brief history of synthetic biology. *Nat Rev Micro* **2014**, *12*, 381–390.

(4) Kelly, C. L.; Liu, Z.; Yoshihara, A.; Jenkinson, S. F.; Wormald, M. R.; Otero, J.; Estévez, A.; Kato, A.; Marqvorsen, M. H. S.; Fleet, G. W. J.; Estévez, R. J.; Izumori, K.; Heap, J. T. Synthetic Chemical Inducers and Genetic Decoupling Enable Orthogonal Control of the rhaBAD Promoter. *ACS Synthetic Biology* **2016**, *5*, 1136–1145.

(5) Wan, X.; Marsafari, M.; Xu, P. Engineering metabolite-responsive transcriptional factors to sense small molecules in eukaryotes: current state and perspectives. *Microbial Cell Factories* **2019**, *18*, 61.

(6) Shimizu-Sato, S.; Huq, E.; Tepperman, J. M.; Quail, P. H. A light-switchable gene promoter system. *Nature Biotechnology* **2002**, *20*, 1041–1044.

(7) Toda, S.; Blauch, L. R.; Tang, S. K. Y.; Morsut, L.; Lim, W. A. Programming self-organizing multicellular structures with synthetic cell-cell signaling. *Science* **2018**, *361*, eaat0271.

(8) Greber, D.; Fussenegger, M. An engineered mammalian band-pass network. *Nucleic Acids Research* **2010**, *38*, e174–e174.

(9) Johnson, M. B.; March, A. R.; Morsut, L. Engineering multicellular systems: using

synthetic biology to control tissue self-organization. *Current opinion in biomedical engineering* **2017**, *4*, 163–173, 29308442[pmid] PMC5749256[pmcid].

(10) Derakhshandeh, H.; Kashaf, S. S.; Aghabaglou, F.; Ghanavati, I. O.; Tamayol, A. Smart Bandages: The Future of Wound Care. *Trends in Biotechnology* **2018**, *36*, 1259–1274.

(11) Acar, M.; Mettetal, J. T.; Van Oudenaarden, A. Stochastic switching as a survival strategy in fluctuating environments. *Nature Genetics* **2008**, *40*, 471–475.

(12) Chen, Y. J.; Groves, B.; Muscat, R. A.; Seelig, G. DNA nanotechnology from the test tube to the cell. *Nature Nanotechnology* **2015**, *10*, 748–760.

(13) Douglas, S. M.; Bachelet, I.; Church, G. M. A logic-gated nanorobot for targeted transport of molecular payloads. *Science* **2012**, *335*, 831–834.

(14) Li, S. et al. A DNA nanorobot functions as a cancer therapeutic in response to a molecular trigger in vivo. *Nature Biotechnology* **2018**, *36*, 258–264.

(15) Freeman, R.; Stephanopoulos, N.; Álvarez, Z.; Lewis, J. A.; Sur, S.; Serrano, C. M.; Boekhoven, J.; Lee, S. S.; Stupp, S. I. Instructing cells with programmable peptide DNA hybrids. *Nature Communications* **2017**, *8*, 15982.

(16) Bhatia, D.; Arumugam, S.; Nasilowski, M.; Joshi, H.; Wunder, C.; Chambon, V.; Prakash, V.; Grazon, C.; Nadal, B.; Maiti, P. K.; Johannes, L.; Dubertret, B.; Krishnan, Y. Quantum dot-loaded monofunctionalized DNA icosahedra for single-particle tracking of endocytic pathways. *Nature Nanotechnology* **2016**, *11*, 1112–1119.

(17) Rudchenko, M.; Taylor, S.; Pallavi, P.; Dechkovskaia, A.; Khan, S.; Butler, V. P.; Rudchenko, S.; Stojanovic, M. N. Autonomous molecular cascades for evaluation of cell surfaces. *Nature Nanotechnology* **2013**, *8*, 580–586.

(18) You, M.; Zhu, G.; Chen, T.; Donovan, M. J.; Tan, W. Programmable and multiparameter DNA-based logic platform for cancer recognition and targeted therapy. *Journal of the American Chemical Society* **2015**, *137*, 667–674.

(19) Song, T.; Shah, S.; Bui, H.; Garg, S.; Eshra, A.; Fu, D.; Yang, M.; Mokhtar, R.; Reif, J. Programming DNA-Based Biomolecular Reaction Networks on Cancer Cell Membranes. *Journal of the American Chemical Society* **2019**, *141*, 16539–16543.

(20) Rinaudo, K.; Bleris, L.; Maddamsetti, R.; Subramanian, S.; Weiss, R.; Benenson, Y. A universal RNAi-based logic evaluator that operates in mammalian cells. *Nature Biotechnology* **2007**, *25*, 795–801.

(21) Chatterjee, G.; Chen, Y. J.; Seelig, G. Nucleic Acid Strand Displacement with Synthetic mRNA Inputs in Living Mammalian Cells. *ACS Synthetic Biology* **2018**, *7*, 2737–2741.

(22) Lentini, R.; Santero, S. P.; Chizzolini, F.; Cecchi, D.; Fontana, J.; Marchioretto, M.; Del Bianco, C.; Terrell, J. L.; Spencer, A. C.; Martini, L.; Forlin, M.; Assfalg, M.; Serra, M. D.; Bentley, W. E.; Mansy, S. S. Integrating artificial with natural cells to translate chemical messages that direct E. coli behaviour. *Nature Communications* **2014**, *5*, 4012.

(23) Schwarz-Schilling, M.; Aufinger, L.; Mückl, A.; Simmel, F. C. Chemical communication between bacteria and cell-free gene expression systems within linear chains of emulsion droplets. *Integrative Biology (United Kingdom)* **2016**, *8*, 564–570.

(24) Lentini, R.; Martín, N. Y.; Forlin, M.; Belmonte, L.; Fontana, J.; Cornella, M.; Martini, L.; Tamburini, S.; Bentley, W. E.; Jousson, O.; Mansy, S. S. Two-Way Chemical Communication between Artificial and Natural Cells. *ACS Central Science* **2017**, *3*, 117–123.

(25) Urtel, G.; Van Der Hofstadt, M.; Galas, J. C.; Estevez-Torres, A. REXPAR: An Isother-

mal Amplification Scheme That Is Robust to Autocatalytic Parasites. *Biochemistry* **2019**, *58*, 2675–2681.

(26) Montagne, K.; Plasson, R.; Sakai, Y.; Fujii, T.; Rondelez, Y. Programming an in vitro DNA oscillator using a molecular networking strategy. *Mol Syst Biol* **2011**, *7*, 466, 10.1038/msb.2010.120.

(27) Van Der Hofstadt, M.; Gines, G.; Galas, J.-C.; Estevez-Torres, A. In *DNA- and RNA-Based Computing Systems*; Evgeny, K., Ed.; John Wiley & Sons, in press.

(28) Fujii, T.; Rondelez, Y. Predator-Prey Molecular Ecosystems. *ACS Nano* **2013**, *7*, 27–34.

(29) Padirac, A.; Fujii, T.; Rondelez, Y. Quencher-free multiplexed monitoring of DNA reaction circuits. *Nucleic Acids Research* **2012**, *40*, e118–e118.

(30) Montagne, K.; Gines, G.; Fujii, T.; Rondelez, Y. Boosting functionality of synthetic DNA circuits with tailored deactivation. *Nature Communications* **2016**, *7*, 13474.

(31) Padirac, A.; Fujii, T.; Estevez-Torres, A.; Rondelez, Y. Spatial Waves in Synthetic Biochemical Networks. *Journal of the American Chemical Society* **2013**, *135*, 14586–14592, doi: 10.1021/ja403584p.

(32) Zadorin, A. S.; Rondelez, Y.; Gines, G.; Dilhas, V.; Urtel, G.; Zambrano, A.; Galas, J. C.; Estevez-Torres, A. Synthesis and materialization of a reaction-diffusion French flag pattern. *Nature Chemistry* **2017**, *9*, 990–996.

(33) Urtel, G.; Estevez-Torres, A.; Galas, J.-C. DNA-based long-lived reaction–diffusion patterning in a host hydrogel. *Soft Matter* **2019**, *15*, 9343–9351.

(34) Baccouche, A.; Montagne, K.; Padirac, A.; Fujii, T.; Rondelez, Y. Dynamic DNA-toolbox reaction circuits: A walkthrough. *Methods* **2014**, *67*, 234–249.

(35) Xiang, X.-Y.; Yang, X.-C.; Su, J.; Kang, J.-S.; Wu, Y.; Xue, Y.-N.; Dong, Y.-T.; Sun, L.-K. Inhibition of autophagic flux by ROS promotes apoptosis during DTT-induced ER/oxidative stress in HeLa cells. *Oncology Reports* **2016**, *35*, 3471–3479.

(36) Zhao, Q.; Matson, S.; Herrera, C. J.; Fisher, E.; Yu, H.; Krieg, A. M. Comparison of Cellular Binding and Uptake of Antisense Phosphodiester, Phosphorothioate, and Mixed Phosphorothioate and Methylphosphonate Oligonucleotides. *Antisense Research and Development* **1993**, *3*, 53–66.

(37) Nödling, A. R.; Mills, E. M.; Li, X.; Cardella, D.; Sayers, E. J.; Wu, S.-H.; Jones, A. T.; Luk, L. Y. P.; Tsai, Y.-H. Cyanine dye mediated mitochondrial targeting enhances the anti-cancer activity of small-molecule cargoes. *Chemical Communications* **2020**,

(38) Fern, J.; Schulman, R. Design and Characterization of DNA Strand-Displacement Circuits in Serum-Supplemented Cell Medium. *ACS Synthetic Biology* **2017**, *6*, 1774–1783.

(39) Lundin, K. E.; Gissberg, O.; Smith, C. E. Oligonucleotide Therapies: The Past and the Present. *Human Gene Therapy* **2015**, *26*, 475–485.

(40) Senoussi, A.; Vyborna, Y.; Berthoumieux, H.; Galas, J.-C.; Estevez-Torres, A. In *Out-of-equilibrium supramolecular systems and materials*; Giuseppone, N., Walther, A., Eds.; Wiley-VCH, in press.

(41) Gines, G.; Menezes, R.; Nara, K.; Kirstetter, A.-S.; Taly, V.; Rondelez, Y. Isothermal digital detection of microRNAs using background-free molecular circuit. *Science Advances* **2020**, *6*.

(42) Guo, S. et al. Engineered Living Materials Based on Adhesin-Mediated Trapping of Programmable Cells. *ACS Synthetic Biology* **2020**, *9*, 475–485.

(43) Zadeh, J. N.; Steenberg, C. D.; Bois, J. S.; Wolfe, B. R.; Pierce, M. B.; Khan, A. R.;

Dirks, R. M.; Pierce, N. A. NUPACK: Analysis and design of nucleic acid systems. *Journal of Computational Chemistry* **2011**, *32*, 170–173.

(44) Wakamatsu, T.; Kitamura, Y.; Kotera, Y.; Nakagawa, N.; Kuramitsu, S.; Masui, R. Structure of RecJ exonuclease defines its specificity for single-stranded DNA. *J Biol Chem* **2010**, *285*, 9762–9.